Communications

Ligand-Clustered "Patchy" Nanoparticles for Modulated Cellular Uptake and In Vivo Tumor Targeting**

Zhiyong Poon, Shujun Chen, Amanda C. Engler, Hyung-il Lee, Evrim Atas, Geoffrey von Maltzahn, Sangeeta N. Bhatia, and Paula T. Hammond

Many biological systems interact through multiple simultaneous interactions.[1–3] While it is well acknowledged that, on the macroscale, these multivalent interactions strongly influence ligand–receptor binding kinetics and the biological responses they govern, the microscale patterning of ligands on substrates can also have a profound effect on multivalent kinetics and are able to further modulate biological signaling.[4] In particular, ligand–receptor clusters can substantially increase interactions between cell and substrate; not only the valency, but spatial factors such as branching mode and the localized clustering of groups are important[5–7] in influencing binding and downstream signaling processes.[8,9] Still, despite the prevalence of patterned ligand presentation found in cell biology and its demonstrated significance on 2D tissue engineering formats,[10,11] it remains largely unappreciated in the design of nanoparticle synthetic systems intended to interact with cells.

Traditionally, ligands have been attached in moderate to large quantities to liposomes, inorganic nanoparticles, and linear–linear block copolymer micelles;[12,13] however, typically they are presented in a randomly distributed fashion across the nanoparticle surface from a linear tether, typically polyethylene glycol (PEG), in a structure that does not enable manipulation of ligands in specific groupings with control of cluster group size and spacing. We hypothesized that precise control over the elements promoting and controlling multivalent presentation on targeted therapeutic carriers could enhance the efficacy and specificity of targeted delivery. To test this hypothesis, scaffolds that are able to localize a variable number of ligands within confined regions are required; this requirement cannot be satisfied by traditional material systems used in targeted delivery[14] such as linear–linear block polymers and PEG-functional liposomes. Here, we introduce the use of a systematic and informed linear dendritic design for a new modular polymer delivery system that can generate clustered or patchy presentations of ligand on micellar surfaces.[15] We demonstrate the use of prefunctionalized linear dendritic polymers (LDPs) in forming mixed micelle formulations that present different spatial arrangements of variable sized ligand clusters and examine the targeting efficacy of these formulations in vitro and in vivo. This new approach to ligand presentation on a nanoparticle surface enables the targeting community to probe means of enhancing cell selectivity at low to moderate ligand concentrations with greatly enhanced uptake. It also provides a tool for the exploration of cellular interactions with nanoscale-patterned ligands.

The design of the LDP is based on drug delivery principles, and each component is either fully biodegradable or biocompatible (Figure 1a). Hydrophobic PBLA (poly-benzyl-L-aspartate) forms the polypeptide linear block to which a generation four hydrolytically degradable polyester dendron is attached. The sixteen end branches of the dendron are extended with sixteen short hydrophilic PEG chains. The degree of polymerization of PBLA is approximately 12 and the PEG branches have molecular weights of approximately $600 \, \mathrm{g \, mol^{-1}}$. The well-characterized model ligand folate,[16]

[*] Z. Poon, S. Chen, A. C. Engler, H. Lee, E. Atas, Prof. P. T. Hammond
Department of Chemical Engineering
Massachusetts Institute of Technology
77 Massachusetts Avenue, Cambridge, MA 02139 (USA)
Fax: (+1) 617-258-7577
E-mail: hammond@mit.edu

H. Lee
Department of Chemistry, University of Ulsan
Ulsan 680-749 (Republic of Korea)

G. von Maltzahn, Prof. S. N. Bhatia
Harvard-MIT Division of Health Science and Technology
Massachusetts Institute of Technology (USA)

Supporting information (including experimental details) for this article is available on the WWW under http://dx.doi.org/10.1002/anie.201003445.
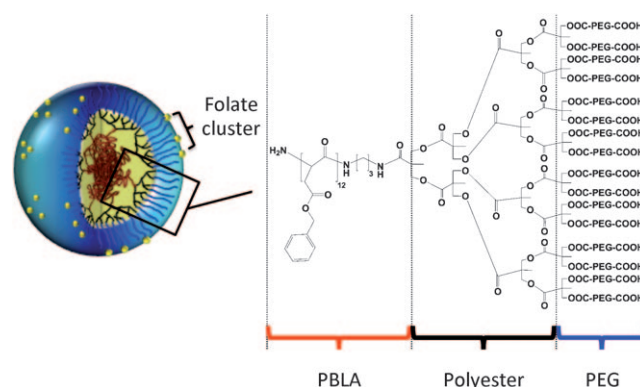

Figure 1. Chemical structure and self-assembly of linear dendritic polymers (LDP). Detailed chemical structure of the non-folate conjugated linear dendritic polymer and illustration of its self-assembly into "patchy" micelles presenting clusters of folate of variable sizes on the surface of the micelle. PBLA = poly(benzyl-L-aspartic acid), PED = polyester dendron, PEG = poly(ethylene glycol).

which is conjugated to the free PEG end through dicyclohexylcarbodiimide/*N*-hydroxysuccinimide (DCC/NHS) chemistries, was selected for this study. Using the model ligand folate, a range of ligand functionalization on the dendron was confirmed by both ^{1}H NMR and UV/Vis spectroscopy, which allows the expression of different folate cluster size ranges on the micelle surface (Figure 2a and Figures S1, S2a, S2c in the
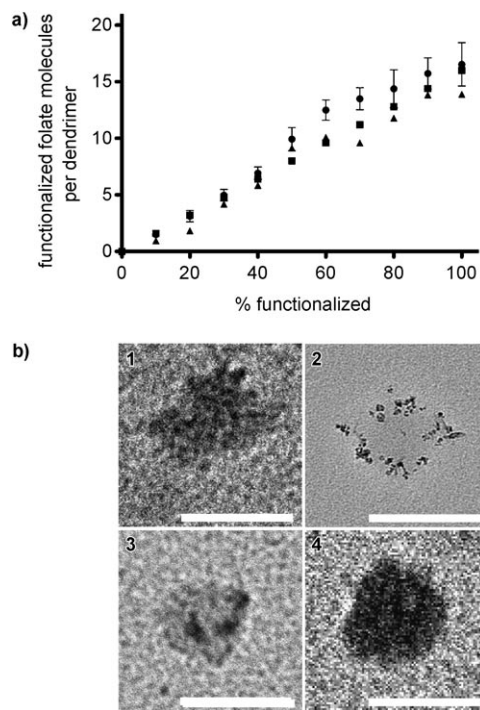

Figure 2. Characterization of LDP mixed micelle system. a) Calculated vs experimental degree of conjugation to dendron. ▲: ^{1}H NMR; ●: UV/Vis; ■: calculated. Experimental values for UV/Vis were calculated using at least three independent sets of measurements (mean ± STD) with free folic acid as the calibration. ^{1}H NMR quantification is described in the Supporting Information. b) TEM images of representative formulations. Clusters of DTPA–Fe^{3+} (DTPA = diethylenetriaminepentaacetic acid dianhydride) on the micelle surface show the formation of mixed micelles. Scale bars = 100 nm. Formulations 10%F–100%mix (1), 20%F–60%mix (2), 30%F–40%mix (3), and 30%F–100%mix (4) are shown.

Supporting Information). The ability of the LDP system to form mixed micelles was confirmed by TEM and FRET (Figure S2d). TEM analysis using Fe^{3+} in the place of folate allow visualization of groupings of "ligands" on the surface of the micelle (Figure 2b).

Using a series of linear dendritic polymers functionalized with 0% to 100% folate groups on the pegylated dendron (0%F to 100%F), we assembled mixed micelles of folate-functionalized polymer with non-functionalized polymer. The resulting micelles present statistically similar amounts of folate but in different cluster arrangements (Figure S2). A series of eight micelle formulations were used: the untargeted control containing unfunctionalized LDP (0%F) used as 100% of the micelle, 0%F–100%mix; and 10%F–100%mix, 20%F–60%mix, 30%F–40%mix, 40%F–30%mix, 60%F–

20%, 70%F–20%mix, and 100%F–10%mix are micelle formulations that present stochastic cluster sizes of, on average, 1.5, 3.1, 5.0, 6.9, 12.5, 13.5, and 16.5 folate groups per cluster (Figure S2c). Micelle presenting folates have an average of 2000–2400 groups per micelle and UV/Vis data show statistically similar numbers of folate by one way ANOVA analysis between the different groups at the 95% confidence interval (Table 1). All micelles were 80–90 nm in size. Micelles that present the same amount, but have different spatial arrangements of folate in variable sized clusters, allow meaningful comparisons to be made to determine the effect of folate spatial presentation on cellular internalization.

We used KB[17] cells to evaluate targeting and binding of the micelles to folate receptors that are overexpressed on the cell surface. After a 24 h period of incubation, there was a clear optimum in folate cluster size. The highest cell associated fluorescence was observed for cells incubated with the 20%F–60%mix formulation (Figure 3a). The measured EC50 (concentration producing 50% binding) was observed to be the lowest for the 20%F–60%mix micelle (Figure 3c). We approximated the apparent dissociation

Table 1: Summary of the eight micelle formulations used in this study.[a]

Micelle	Effective diameter [nm]	PDI	Zeta potential [mv]	Folate molecules per micelle
0%F–100%mix	74 ± 1	1.16	−24 ± 3.4	0
10%F–100%mix				1900 ± 250
20%F–60%mix				2200 ± 260
30%F–40%mix				2400 ± 520
40%F–30%mix	90 ± 4	1.2 ± 0.1	−20 ± 0.8	2260 ± 390
60%F–20%mix				2400 ± 400
70%F–20%mix				3100 ± 700
100%F–10%mix				1900 ± 450

[a] 0%F–100%mix is the untargeted control, all other formulations present similar amounts (not statistically different by one-way ANOVA analysis at the 95% CI) of folate but in different cluster sizes and arrangements. Total number of folate presented per micelle (mean ± STD) is calculated based on at least three sets of data (UV/Vis) using an approximate micelle aggregation number of 1000 (based on measured diameters and estimates of LDP unimer dimensions from Materials Studio). Average micelle diameters and zeta potentials are given in mean ± STD of the averages of at least ten individual measurements per micelle. Additional information on diameter, zeta potential information, and folate presentation are shown in Figures S3 and S2b.

Table 2: Apparent K_D, k_{on}, and k_{off} values for the targeted formulations.[a]

Micelle	K_D [M]	K_{off} [s⁻¹]	K_{on} [M⁻¹ s⁻¹]
10%F–100%mix	$(3.1 ± 0.5) × 10^{-9}$	$(1.2 ± 0.3) × 10^{-3}$	$3.8 × 10^5$
20%F–60%mix	$(1.7 ± 0.3) × 10^{-11}$	$(1.6 ± 0.4) × 10^{-5}$	$9.6 × 10^5$
30%F–40%mix	$(4.0 ± 1.2) × 10^{-11}$	$(3.0 ± 1.8) × 10^{-5}$	$7.4 × 10^5$
40%F–30%mix	$(9.2 ± 1.8) × 10^{-11}$	$(8.3 ± 0.3) × 10^{-5}$	$9.0 × 10^5$
60%F–20%mix	$(2.3 ± 0.8) × 10^{-10}$	$(4.0 ± 1.2) × 10^{-4}$	$1.8 × 10^6$
70%F–20%mix	$(1.5 ± 0.8) × 10^{-10}$	$(1.2 ± 0.7) × 10^{-3}$	$7.4 × 10^5$
100%F–10%mix	$(3.3 ± 0.6) × 10^{-9}$	$(9.3 ± 1.9) × 10^{-4}$	$2.8 × 10^5$

[a] K_D and k_{off} were determined experimentally (at least three sets of independent data each), K_{on} was calculated as $k_{on} = k_{off}/K_D$ using mean k_{off} and K_D values.
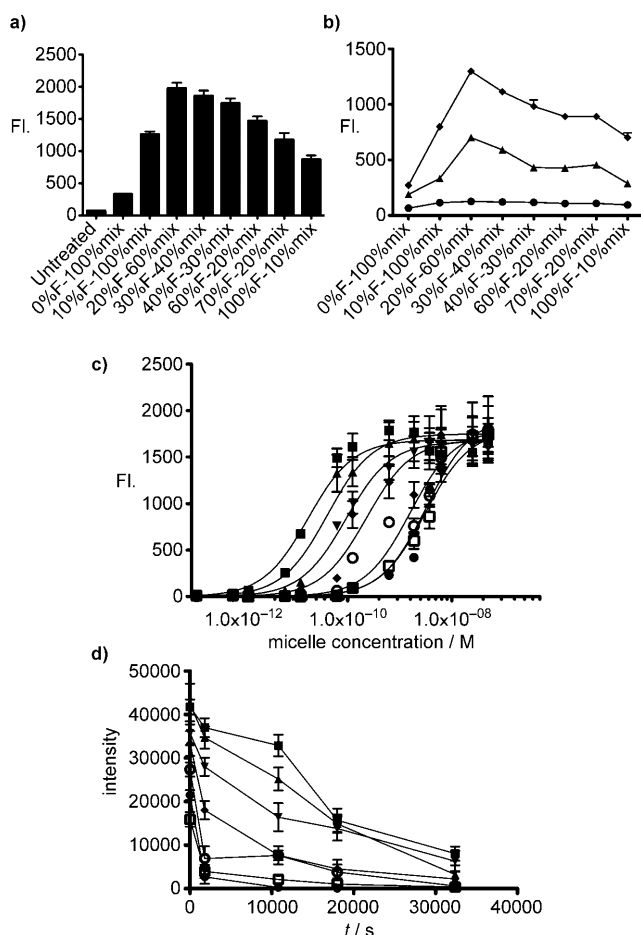
Figure 3. In vitro evaluation of patchy micelles on KB (folate receptor, FR+) and A375 (FR−) cells. a) KB cell-associated fluorescence (Fl.) after 24 h of incubation with micelle formulations. Highest fluorescence was measured from KB cells incubated with 20%F–60%mix formulation (Figure S4a). b) Measured cell-associated fluorescence (Fl.) of KB cells at 5 min (●), 1 h (▲), and 6 h (◆) post incubation. Increase in cell-associated fluorescence between 1 h and 6 h are similar for all targeted formulations, indicating that rate of endocytosis is unaffected by folate presentation. c) The binding avidity (K_D) measured for targeted formulations (●: 10%F–100%mix; ■: 20%F–60%mix; ▲: 30%F–40%mix; ▼: 40%F–30%mix; ◆: 60%F–20%mix; ○: 70%F–20%mix; □: 100%F–10%mix) shows highest avidity with 20%F–60%mix. d) The measured rate of decrease in micelle fluorescence after fixed KB cells pre-incubated to equilibrium with micelles was re-suspended in PBS (phosphate buffered saline). Nonlinear regression analysis using a one-phase exponential decay model gives the apparent dissociation rate constant of micelles from membrane receptors (k_{off}). Calculated values for targeted formulations show the longest dissociation rate with 20%F–60%mix. K_D, k_{off}, and k_{on} values are shown in Table 2. All graphs shown are made with measurements on $n > 3$ independent experiments and are given in mean ± SEM values. Individual flow cytometry measurements were averaged out of 10 000 events.

constants of the tested micelles (K_D) by fitting a binding model for site-specific binding to the experimental data. The apparent micelle K_D are given in Table 2. The measured dissociation rate constant (k_{off}) of the different micelles also show that the optimal 20%F–60%mix formulation had the longest dissociation time (2×10^{-5} s^{-1}; Figure 3d, Table 2).

The rate of micelle association was calculated as $k_{on} = k_{off}/K_D$ and was found to be less than 1 order of magnitude apart (Table 2). Confocal analysis and competitive binding experiments confirmed that binding and targeting are folate receptor (FR) mediated and that the mechanism for internalization of targeted LDP is dependent on both energy driven endocytosis and the presence of folate receptors (Figure S5).

To further account for the observed differences in cell targeting, we examined the cell uptake post incubation with micelles as a measure of the kinetics of internalization through the folate receptor (Figure 3b). After a 1 h binding time for internalization, the rate of change in cell-associated fluorescence is not significantly different for all formulations between 1 h and 6 h, indicating that the actual mechanisms of folate internalization are not dependent on ligand presentation; however, the relative levels of cell fluorescence show a strong relationship with their respective binding avidities. All micelle formulations exhibited saturation uptake kinetics at longer time points, suggesting that equilibrium between uptake and secretion was reached by 20 h (Figure S5c). These observations indicate that the enhanced cell targeting of micelles with optimal folate cluster presentation is attributed to having more micelles bind for longer times on the cell surface, which increases the chance for endocytosis.

We estimate that the dendritic element of the LDP has a head group area of 50 to 80 nm^2 and the FR is a protein of ca. 30 kDa that projects a binding area of ca. 13 nm^2 into extracellular space.[18] Examinations of cell membranes that overexpress FR indicate that the FR molecules exist in nanoscale clusters on lipid rafts, with a majority of those clusters consisting of three or more FR molecules.[19–23] Given the available binding space afforded by each dendron, the range of folate–FR interactions that can occur is between 0 and 6, corresponding to LDP conjugated with up to 40% folate. If we were to treat each dendron as a binding entity, LDP–10%F (1.5 ± 0.4 folates/dendron) would bind most weakly to FR clusters and the binding energies of LDP–20%F (3.1 ± 0.9), LDP–30% (5.0 ± 0.9), and LDP–40%F (6.9 ± 0.9) would be greater. Once past the allowable number of ligand–receptor binding events ($>$LDP–50%F, 9.9 ± 1.8 folates/dendron) within the binding space, the presence of excess ligands clustered in a small binding area would result in steric binding interference, lowering the binding energy.[24]

The cooperativity of this multivalent system can also be helpful in understanding binding effects. This is a negatively cooperative system, as $K_{multivalent} < (K_{monovalent})^{\alpha N}$, where K is the dissociation constant, N is the total number of ligands, and α is the degree of cooperativity (Table 2).[8] In negatively cooperative systems, each successive ligand interaction with a receptor is less favorable than the previous interaction. The calculated degree of cooperativity shows that all formulations were negatively cooperative ($\alpha < 1$ for all formulations), but among the tested micelles, 20%F–60%mix had the highest α, indicating that it is possible to achieve a particular ligand configuration that optimizes the use of each ligand, making the system less negatively cooperative (α closer to 1).

To investigate the significance of cluster presentation in vivo, we delivered formulations 0%F–100%mix, 20%F–60%mix, 60%F–20%mix, and 70%F–20%mix (blood circu-
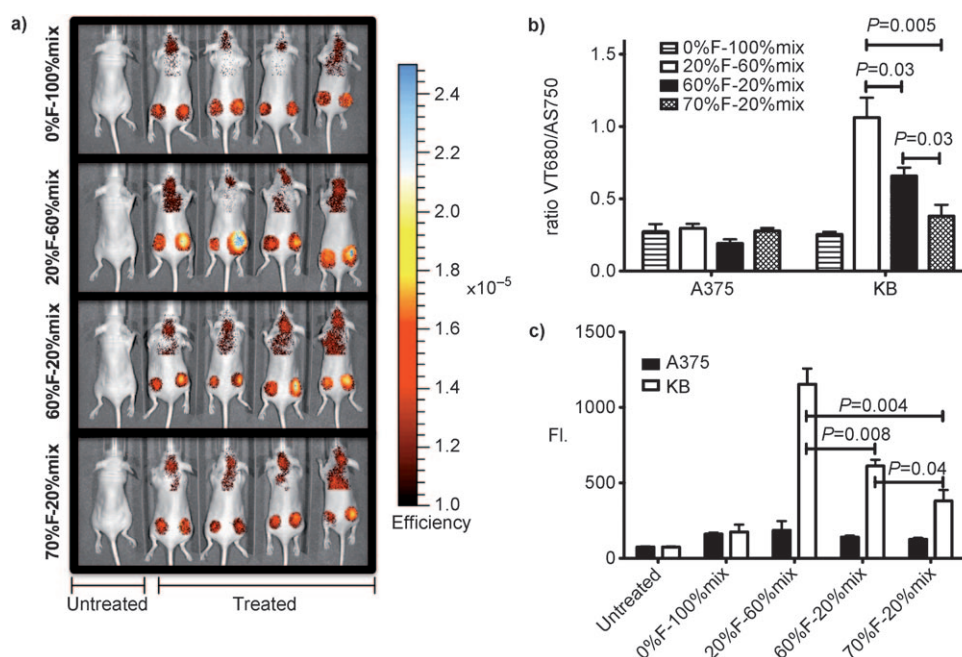
Figure 4. In vivo evaluation of patchy micelles on nude mice bearing two different tumors (right flank: KB, left flank: A375). a) Fluorescence 3D optical imaging of tumored nude mice 48 h after injection with different formulation micelles. Only fluorescence from tumors and a nontumored region of the mice (upper torso) is shown. A side-by-side comparison of VT680 and AngioSence750 fluorescence on the same scale is also shown in Figure S7 to allow identification of the tumors. b) Normalized tumor fluorescence (VivoTag680(VT680)/AngioSense750(AS750)) of tumors ($n=4$) showing the highest in vivo targeting with 20%F–60%mix micelles. Raw fluorescence data is an average of the fluorescence in the region of interest, given in units of efficiency. Ratios are 0.27 ± 0.11, 0.30 ± 0.06, 0.19 ± 0.06, and 0.28 ± 0.04 for A375 tumors and 0.25 ± 0.04, 1.06 ± 0.27, 0.66 ± 0.11, and 0.38 ± 0.16 for KB tumors (0%F–100%mix, 20%F–60%mix, 60%F–20%mix, and 70%F–20%mix, respectively). c) Mean cell-associated micelle fluorescence (Fl.) for cells gated in Q1+Q3 (see Figure S7) are 160 ± 16, 185 ± 104, 140 ± 17, and 126 ± 15 for A375 tumors and 175 ± 84, 1153 ± 104, 611 ± 71, and 380 ± 126 for KB tumors (0%F–100%mix, 20%F–60%mix, 60%F–20%mix, and 70%F–20%mix, respectively). All data is given in mean $\pm$ SEM.

lation half lives 15–20 h; Figure S6) to nude mice bearing KB (FR+) and A375 (FR–) tumors. Figure 4 and Figure S7 show the results from imaging 48 h after injection of micelles. The highest normalized micelle fluorescence was observed for KB tumors in mice injected with 20%F–60%mix. Ratios for the untargeted formulations and all targeted formulations against A375 tumors were found to be within error. To further localize the micelles within the tumor tissue, flow cytometry analysis was performed on tumor cells isolated from whole tumors. We note that the similar trend in data for flow cytometry analysis and 3-D optical imaging show that at the 48 h time point, the majority of the fluorescence accounted for with tumor imaging were from micelles that have been internalized into tumor cells through specific (substantial) or non-specific mechanisms (minimal). The intravenously delivered targeted formulations were able to substantially internalize in live tumor cells in vivo, resulting in a higher population of cells with a higher fluorescence. Optimal clustering of folate also played an important role in enhancing multivalent folate–FR cluster interactions, with the 20%F–60%mix formulation showing the highest level of fluorescence amongst targeted formulations ($P < 0.05$ for all analyses comparing 20%F–60%mix, 60%F–20%mix and 70%F–20%mix).

We have shown that ligand presentation in cluster arrangements is a viable design parameter for increasing the efficacy of targeted nanoparticles. In our experiments, cluster arrangement of folate in an optimal size of ca. 3 enhanced uptake of nanoparticles owing to the resultant higher avidity and longer residence times on the cell membrane. This plays a critical role for in vivo targeting where the percentage of intravenously delivered nanoparticles that reach tumor sites by EPR (enhanced permeation and retention) is often less than $10\%\,\text{ID}\,\text{g}^{-1}$,[25] resulting in a low concentration of nanoparticles in the tumor interstitial made available for uptake by tumor cells. To achieve substantial levels of therapy, the avidity of the delivered nanoparticle must be high enough to be able to bind to receptors under such conditions. The results presented here suggest that a shift in focus in molecularly targeted nanocarriers from ligand density to the specific manipulation of ligand cluster presentation may have important implications on cell targeting and can guide the development of more effective targeted delivery systems. It has also been demonstrated that the modular and tunable nature of the linear–dendritic platform can provide a useful probe to examine the importance of ligand–cluster arrangements for cellular interactions.

[1] P. I. Kitov, J. M. Sadowska, G. Mulvey, G. D. Armstrong, H. Ling, N. S. Pannu, R. J. Read, D. R. Bundle, *Nature* **2000**, *403*, 669.

[2] M. Mourez, R. S. Kane, J. Mogridge, S. Metallo, P. Deschatelets, B. R. Sellman, G. M. Whitesides, R. J. Collier, *Nat. Biotechnol.* **2001**, *19*, 958.

[3] X. Montet, M. Funovics, K. Montet-Abou, R. Weissleder, L. Josephson, *J. Med. Chem.* **2006**, *49*, 6087.

[4] C. W. Cairo, J. E. Gestwicki, M. Kanai, L. L. Kiessling, *J. Am. Chem. Soc.* **2002**, *124*, 1615.

[5] S. André, H. Kaltner, T. Furuike, S. I. Nishimura, H. J. Gabius, *Bioconjugate Chem.* **2004**, *15*, 87.

[6] E. A. L. Biessen, F. Noorman, M. E. van Teijlingen, J. Kuiper, M. Barrett-Bergshoeff, M. K. Bijsterbosch, D. C. Rijken, T. J. van Berkel, *J. Biol. Chem.* **1996**, *271*, 28024.

[7] A. David, P. Kopeckova, T. Minko, A. Rubinstein, J. Kopecek, *Eur. J. Cancer* **2004**, *40*, 148.

[8] M. Mammen, S.-K. Chio, G. M. Whitesides, *Angew. Chem.* **1998**, *110*, 2908; *Angew. Chem. Int. Ed.* **1998**, *37*, 2754.

[9] J. Schlessinger, *Cell* **2000**, *103*, 211.

[10] G. Maheshwari, G. Brown, D. A. Lauffenburger, A. Wells, L. G. Griffith, *J. Cell Sci.* **2000**, *113*, 1677.

[11] L. Y. Koo, D. J. Irvine, A. M. Mayes, D. A. Lauffenburger, L. G. Griffith, *J. Cell Sci.* **2002**, *115*, 1423.

[12] S. Azarmi, W. H. Roa, R. Lobenberg, *Adv. Drug Delivery Rev.* **2008**, *60*, 863.

[13] R. Duncan, *Nat. Rev. Cancer* **2006**, *6*, 688.

[14] R. Duncan, *Nat. Rev. Drug Discovery* **2003**, *2*, 347.

[15] L. Tian, P. T. Hammond, *Chem. Mater.* **2006**, *18*, 3976.

[16] M. D. A. Salazar, M. Ratnam, *Cancer Metastasis Rev.* **2007**, *26*, 141.

[17] Y. Lu, E. Sega, C. P. Leamon, P. S. Low, *Adv. Drug Delivery Rev.* **2004**, *56*, 1161.

[18] J. Holm, S. I. Hansen, M. Hoier-Madsen, H. Birn, P.-E. Helkjaer, *Arch. Biochem. Biophys.* **1999**, *366*, 183.

[19] S. D. Weitman, R. H. Lark, L. R. Coney, D. W. Fort, V. Frasca, V. R. Zurawski, Jr., B. A. Kamen, *Cancer Res.* **1992**, *52*, 3396.

[20] J. J. Turek, C. P. Leamon, P. S. Low, *J. Cell Sci.* **1993**, *106*, 423.

[21] B. A. Kamen, M. T. Wang, A. J. Streckfuss, X. Peryea, R. G. W. Anderson, *J. Biol. Chem.* **1988**, *263*, 13602.

[22] R. J. Lee, P. S. Low, *J. Biol. Chem.* **1994**, *269*, 3198.

[23] S. Hong, P. R. Leroueil, I. J. Majoros, B. G. Orr, J. R. Baker, M. M. Banaszak Holl, *Chem. Biol.* **2007**, *14*, 107.

[24] W. S. Hlavacek, R. G. Posner, A. S. Perelson, *Biophys. J.* **1999**, *76*, 3031.

[25] H. Maeda, J. Wu, T. Sawa, Y. Matsumura, K. Hori, *J. Controlled Release* **2000**, *65*, 271.

[26] M. Pittelkow, R. Lewinsky, J. B. Christensen, *Org. Synth.* **2007**, *84*, 209.

[27] N. Parker, M. J. Turk, E. Westrick, J. D. Lewis, P. S. Low, C. P. Leamon, *Anal. Biochem.* **2005**, *338*, 284.

[28] C. A. Ladino, R. V. J. Chari, L. A. Bourret, N. L. Kedersha, V. S. Goldmacher, *Int. J. Cancer* **1997**, *73*, 859.

Angewandte Chemie

Supporting Information

Ligand-Clustered "Patchy" Nanoparticles for Modulated Cellular Uptake and In Vivo Tumor Targeting**

*Zhiyong Poon, Shujun Chen, Amanda C. Engler, Hyung-il Lee, Evrim Atas, Geoffrey von Maltzahn, Sangeeta N. Bhatia, and Paula T. Hammond**

anie_201003445_sm_miscellaneous_information.pdf

Experimental Section

Synthesis of LDP and its derivatives. We synthesized the LDP according to published protocols[15]. n-dodecyl-L-glutamate was substituted for benzyl-L-aspartic acid (Sigma Aldrich) and the synthesized polymer was characterized with ^{1}H NMR. Folate and labeling agents were conjugated to the LDP dendron using N-boc-1,3-diaminopropane (synthesized according to published protocols[26]) as an intermediate. Detailed information on the synthesis and characterization of the polymer and the assembled micelles is provided in the Supplementary Information section online.

Synthesis of LDP and its derivatives. The LDP used in this study (PBLA$_{12}$-(Generation 4 dendron)Polyester-PEG(600 g/mol)) has a theoretical molecular weight of 14144 g/mol. For stiochiometric folate attachment to LDP, folic acid was activated using DCC/NHS chemistry and this was subsequently reacted with N-boc-1,3-diaminopropane. The resultant molecule (Folate-1,3-diaminopropane-boc) was deprotected with excess trifluoroacetic acid (10X) and purified by precipitation in water. After purification, folate-1,3-diaminopropane-NH$_2$ was reacted in stiochiometric excess with the amount of functional –COOH groups present on the LDP dendron (EDC/NHS) and in the presence of triethylamine to achieve folate functionalization of the dendron to varying percentages. All reactions were done in DMF. After reaction, the polymers were dialyzed in a 10KMWCO dialysis bag for 2 days before lyophilization to yield the product. We determined the degree of folate functionalization using UV-Vis (free folic acid as calibration, adsorption at 290nm) and ^{1}HNMR. We used the following peaks as reference: for folate, the aminobenzoyl moiety at ~6.5ppm (2H) and for LDP, the combined integration of 4.13ppm (d, 16H, -CH$_2$O) and 4.24-4.32ppm (m, 24H, -CH$_2$O) corresponding to the dendritic esters (40H). We chose the dendritic ester peaks as a reference because it is structurally closer to the position of folate on the molecule; these peaks were also used as a reference for ^{1}HNMR analysis during the synthesis of the LDP. N-boc-1,3-diaminopropane-DTPA (Sigma Aldrich) / VT680 (VisEn Medical) were also synthesized using DCC/NHS chemistry and subsequently deprotected to expose the second primary amine for reaction with activated (DCC/NHS) carboxyl PEG on the LDP. Alexa Fluor 488/594/ 647 (Invitrogen) cadaverine were directly labeled on the dendron with EDC/NHS chemistry. The labeling agents were conjugated at a 1:1 LDP:labeling agent molar ratio. After reaction, the products were separated with dialysis (10KMWCO) and purified with a Sephadex G-25 column before lyophilization. Labeled LDP were made by conjugating labeling agents to the dendron of unfunctionalized LDP. A small fixed amount (~5% concentration ratio) of the appropriate labeling LDP was used during self-assembly with the unfunctionalized and folate functionalized LDP to allow tracking of these particles (all conjugation schemes summarized in the methods section). This allows all micelle formulations to be labeled similarly with the dye. During assembly into nanoparticles, the hydrophobic PBLA linear block forms the core, which encapsulates hydrophobic drugs, while the hydrophilic dendritic block forms the shell, presenting folate that targets cell receptors. Self-assembly of these nanoparticles from pre-functionalized LDP enables variable sized folate clusters to be presented on the nanoparticle surface.

Micelle preparation and characterization. Folate conjugated LDP and non-functionalized LDP were mixed in different ratios to create nanoparticles with different folate spatial presentations. The micelles were further labeled either fluorescently or radioactively by incorporation of a small amount of the synthesized LDP-labeling agent; this ensures micelles contain on average a similar amount of fluorescent dye. Micelles containing LDP-DTPA were complexed with ^{111}In (InCl) or Fe^{3+} (FeCl$_3$) in sodium acetate buffer and were purified from the uncomplexed metal ions using a PD-10 salt column (GE healthcare). Micelles were self-assembled using a dialysis method: briefly, the LDP formulations (dissolved in DMF) were placed inside a 10KMWCO dialysis bag (Pierce Chemical) and dialyzed against DI water under sink conditions. DI water was replaced frequently for a total dialysis time of ~24 h. After all DMF was removed, the contents of the dialysis bags were filtered with a 0.2 μm teflon filter before lyophilization and use. Micelles were characterized using dynamic light scattering (CONTIN fit, ZetaPALS), TEM and FRET (AF488 and AF594 are donor-acceptor pairs). An excitation wavelength of 475 nm (AF488 donor excitation) was used and emission was recorded at 630 nm (AF594 acceptor emission). For TEM imaging, micelle solutions were drop-cast onto carbon coated copper grids without any staining. TEM of these micelles was performed on a JEOL 2011 high contrast digital TEM operating at 200KV accelerating voltage. The degree of folate conjugation on LDP was determined using UV-vis spectroscopy (absorption at 290nm).

Free folic acid was used to obtain a standard calibration. Folate surface density was determined using aggregation numbers estimated from LDP (Materials Studio) and micelle dimensions. Addition of folate increased the diameters of the micelles and micelles with the same amount of folate have averaged diameters within ±10 % of each another (Figure 2e). In addition, the zeta potentials of all micelle variations were also constant at ~ -20 ± 5 mV (Supplementary Figure 3). This suggests that the aggregation numbers of the micelles do not change significantly, even when different polymer ratios are used in the formation of the micelles. We estimate that the aggregation numbers are in the order of 10^3 based on data from DLS/TEM and calculations of the size of each individual LDP from Materials Studio®. CMCs measured for all micelles were of the same order of magnitude of 10^{-8}M.

Radiolabeling. Formulations (1mg/mL) containing the LDP-DTPA polymer in PBS were incubated with 200 μCi of ^{111}InCl$_3$ (in 1M sodium acetate buffer) at room temperature for 30 min. The resulting radiolabelled formulations were purified from free ^{111}In by gel filtration through a PD-10 column (GE healthcare) using PBS as the eluting phase.

In vitro experimentation. Human nasopharyngeal carcinoma cells (KB, FR positive)[22, 27] (ATCC), and human melanoma cells (A375, FR negative)[28] (ATCC), were used in our experiments. Folic acid free 1640 RPMI media was bought from Invitrogen, supplemented with 10% fetal bovine serum, 50 units/mL penicillin and 50 units/mL streptomycin. All cells were cultured in this media for at least 4 days before use. For all experiments, cells were scraped, washed, counted and plated as necessary in 24 or 96 well plates and allowed to grow to ~70% confluence. Before use, new media was added following a wash with PBS supplemented with 0.1% BSA. For determining uptake, micelle formulations (0.5mg/mL, AF647 labeled) were added for different incubation times. After incubation, the cells were washed with PBS (x3), trypsinized and re-suspended in PBS (0.1% BSA) for flow cytometry analysis. For binding avidity experiments, a range of micelle formulations at different concentrations were incubated with cells on ice for 1 h, washed with cold PBS to remove unbound ligand and re-suspended in cold PBS for flow cytometry analysis. Polymer concentrations used were above the CMC of 1×10^{-8}M. The degree of specific binding was determined by subtracting the amount of non-specific binding (micelle with no ligand) from total binding. To facilitate analysis, apparent K_D values were calculated by fitting experimental data to a non-linear regression method for a 1:1 single site specific binding model in PRISM (built in model). For dissociation kinetic experiments, cells were fixed in 4% paraformaldehyde, washed with PBS (0.1% BSA) and allowed to bind with micelles for 1 h to allow equilibrium. Following incubation, the cells were centrifuged and re-suspended in fresh buffer without micelles. This cell suspension was constantly stirred and was sampled at several time points thereafter to determine remaining cell fluorescence as a measure of the degree of dissociation of bound micelles. The sampled cells were spun down, washed, lysed and the resultant AF647 fluorescence from the lysed cells was measured using a spectrofluorometer. The decay in fluorescence was plotted against time and the experimental data was fitted to a built-in one phase exponential decay model in PRISM to determine apparent k_{off} values. As Koff and K_D were measured at different temperatures, the calculated rate of association (K_{on}) using equation: $k_{on} = k_{off}/K_D$, are also apparent values and are used to show the K_{on} relationship between different micelles. All flow cytometry analyses were performed on an LSRII (BD Biosciences) system.

For confocal microscopy, cells were grown until 50% confluent on chamber slides and treated with various micelle formulations and transferrin-A488 (when necessary) under different conditions (AF647 labeled). The cells were then washed repeatedly with PBS, fixed with 4% paraformaldehyde, permeabilized with cold ethanol, blocked with 0.1% BSA in PBS and stained with Hoechst (10μg/mL) for 5 min. The fixed cells were then washed again with PBS and examined with a Delta vision confocal microscope (60X).

In vivo experimentation. All in vivo experimentation was carried out under the supervision of the Division of Comparative Medicine, Massachusetts Institute of Technology, and in compliance with the Principles of Laboratory Animal Care of the National Institutes of Health.
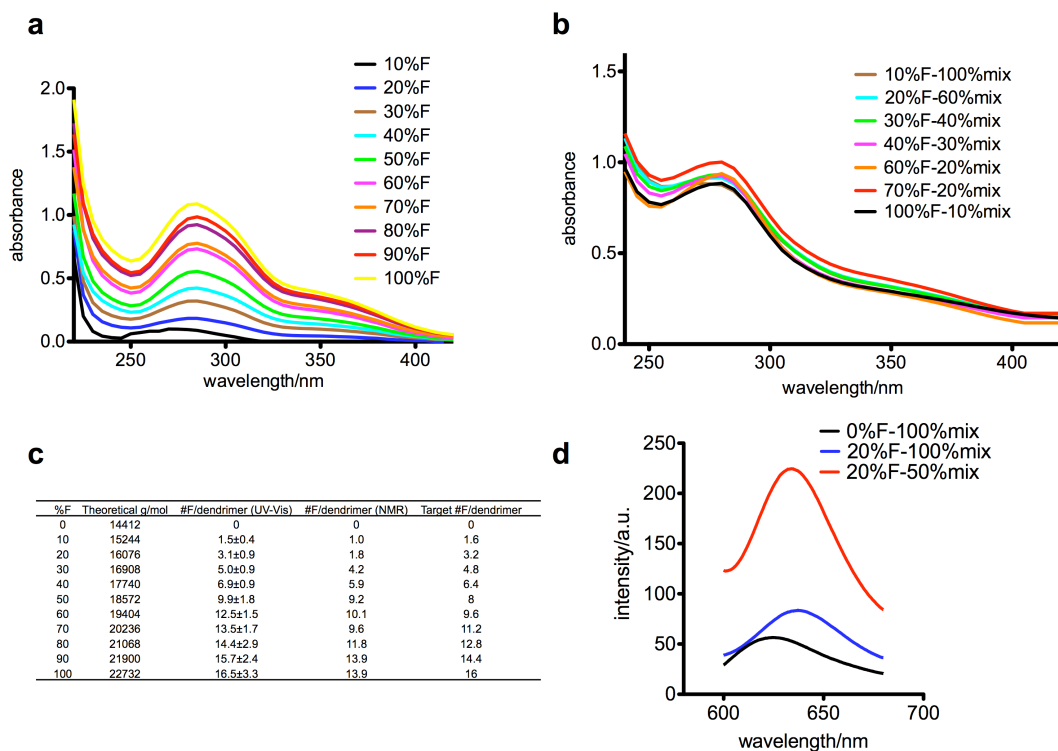
Female nude BALB/c mice (3-4 weeks old, Charles River) were fed a folate deficient diet (Research Diets) for at least a week to achieve plasma folate levels commensurate with humans. Tumors were induced subcutaneously and bilaterally in the hind flanks with 2×10^6 KB/A375 cells. Experimentation began when the tumors developed to ~ 100-200 mm^3 (<10% body weight, <1cm in any dimension). Tumored mice were then separated into random groups and given tail vein injections of labeled formulations (10 mg polymer/kg, 1 injection/formulation/mice). Blood circulation half-lives were determined by the decrease in

radioactivity from blood drawn from the saphenous vein with heparinized capillary tubes. 3-D fluorescence imaging was performed using an IVIS imaging system and mice to be imaged were given an injection of AngioSense750 (0.1mL/mice, 5nmol) 24hrs before imaging. VT680 fluorescence was detected using 675nm/720nm (ex/em) and AngioSense750 was detected using 745/800 (ex/em). For flow cytometry analyses of tumor cells, xenograft whole tumors were minced completely with sterile blades before a mixture of collagenase (II) in RMPI 1640 medium was added (200-250 units of collagenase/mL). The tumor pieces were allowed to incubate at 37°C for 3– 4 hrs with gentle agitation every 30min. At the end of the incubation, cells were filtered through a 0.45μm nylon mesh, washed with PBS (X3) and counter stained with propidium iodide (5μM), washed with PBS and re-suspended. VT680 micelle fluorescence was detected on the LSRII using the APC Cy7 detector.
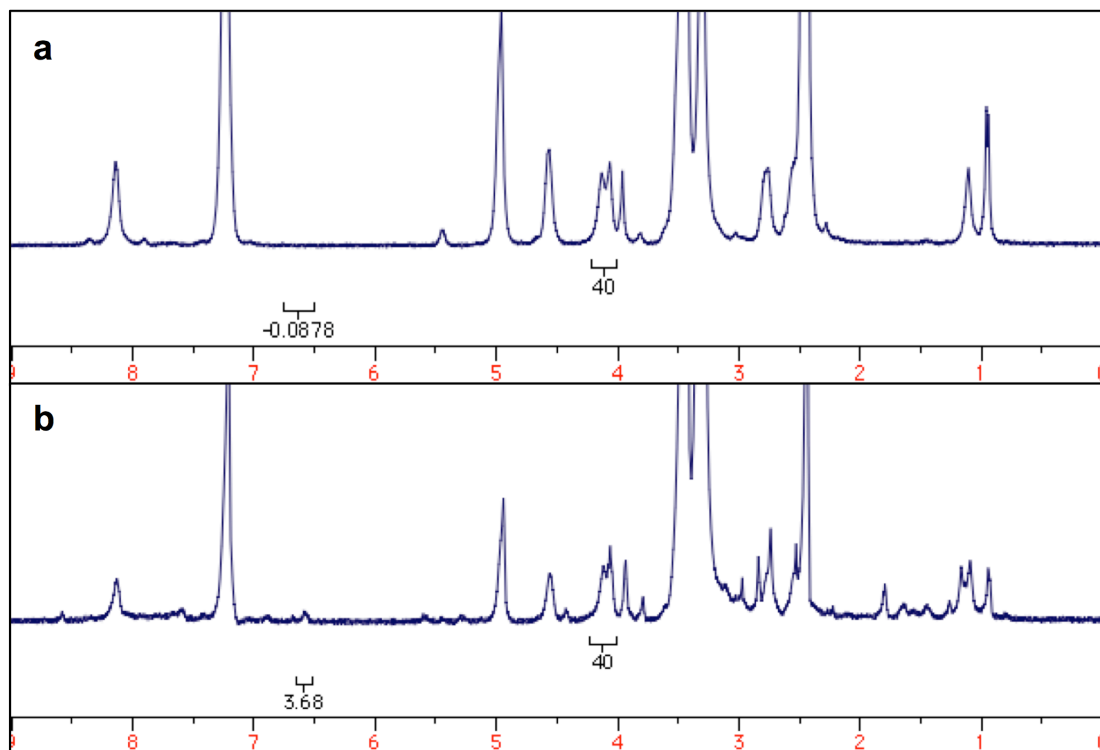
Supplementary Figure 1. Representative ^{1}HNMR spectra of a) LDP and b) LDP-20%F. We used the following peaks as reference: for folate, the aminobenzoyl moiety at ~6.5ppm (2H) and for LDP, the combined integration of 4.13ppm (d, 16H, -CH$_2$O) and 4.24-4.32ppm (m, 24H, -CH$_2$O) corresponding to the dendritic esters (40H).

c)

| %F	Theoretical g/mol	#F/dendrimer (UV-Vis)	#F/dendrimer (NMR)	Target #F/dendrimer
0	14412	0	0	0
10	15244	1.5±0.4	1.0	1.6
20	16076	3.1±0.9	1.8	3.2
30	16908	5.0±0.9	4.2	4.8
40	17740	6.9±0.9	5.9	6.4
50	18572	9.9±1.8	9.2	8
60	19404	12.5±1.5	10.1	9.6
70	20236	13.5±1.7	9.6	11.2
80	21068	14.4±2.9	11.8	12.8
90	21900	15.7±2.4	13.9	14.4
100	22732	16.5±3.3	13.9	16

Supplementary Figure 2. a) UV-vis spectroscopic data for LDP conjugated from 0% to 100% folate on the 16 dendritic ends. Folate was detected at 290nm (absorption). b) Mean UV-Vis spectra of formulations used in this study (n>3 readings). c) Table showing theoretical molecular weights, theoretical and calculated number of folate conjugated per LDP dendron. UV-Vis quantification was done with at least 3 data sets (mean±STD) and ^{1}HNMR was based on a single spectrum. Paper discussion is based on UV-Vis data obtained with free folic acid as calibration (absorption at 290nm). D) FRET showing the formation of mixed micelle prepared with LDP-0% functionalized with AF488 and LDP-20% functionalized with AF594 and diluted down to concentrations (~1 µM) just above their CMCs (~10^{-8}M). Energy transfer between AF488 and AF594 occurs across distances of ~5 nm. Detection of emission at 630 nm confirmed the formation of mixed micelles.
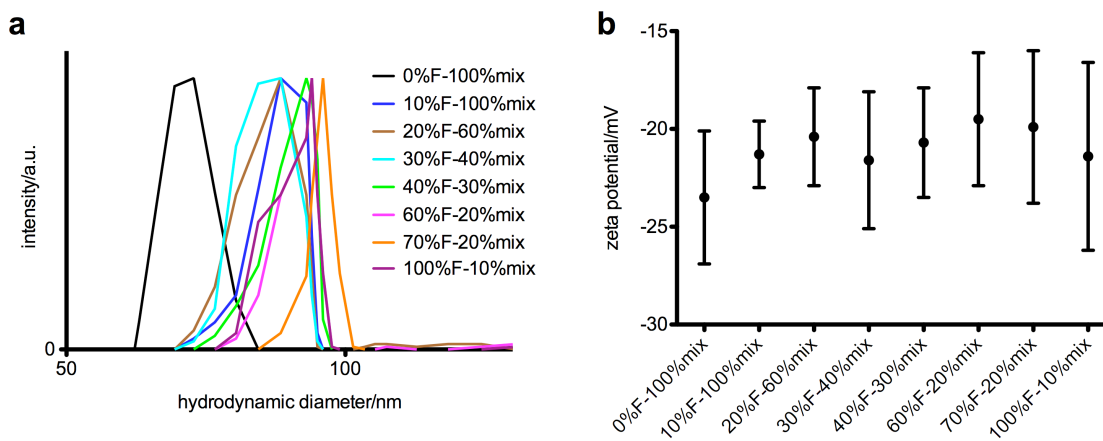

Supplementary Figure 3. Hydrodynamic diameters measured with dynamic light scattering (COUNTIN fit) (a) and zeta potentials (b) of micelles used in this study.
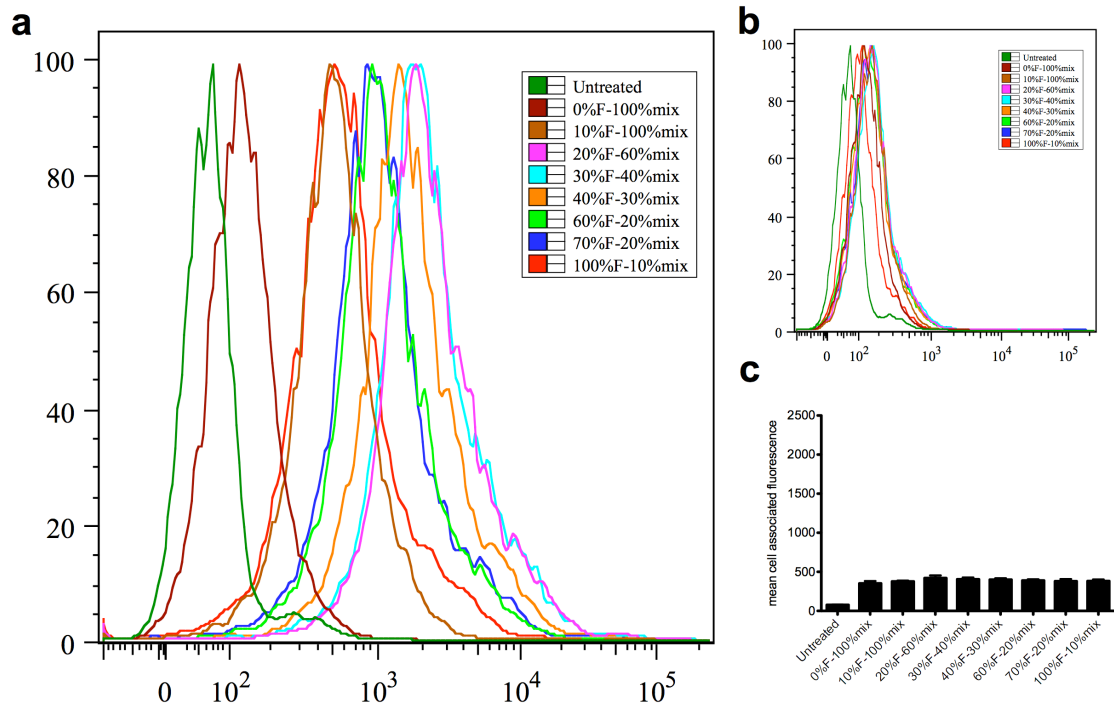
Supplementary Figure 4. Histograms of flow cytometry analysis for KB (a) and A375 (b) cells incubated with micelle formulations for 24 h. c) A375 cell associated fluorescence was within the same range for cells incubated with all formulations (Supplementary Figure 4b).
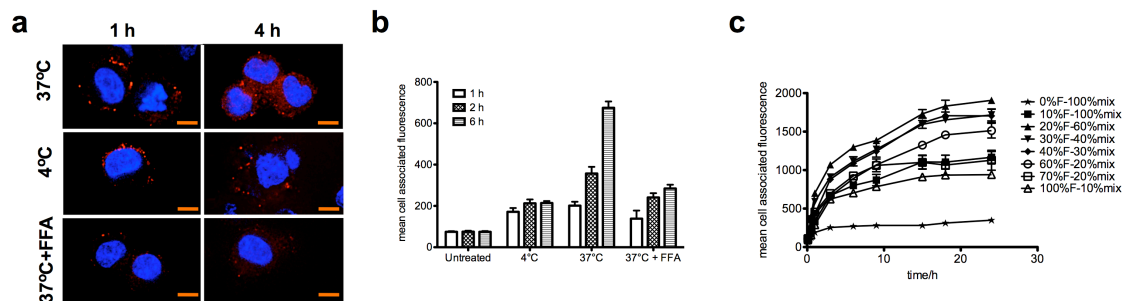
Supplementary Figure 5. a) Confocal microscope analysis (60X) of fixed KB cells after different treatments showing position of folate targeted micelles (red). Cells are counterstained with Hoechst to highlight position of nuclei. After 1 h of incubation, cell associated fluorescence is mainly attributed to membrane bound micelles. Internalized micelles after 1 h of incubation accounts for most of the cell associated fluorescence from micelles. No micelle fluorescence was detected inside the cell when incubated at a lower temperature. Competition with FFA (free folic acid 1μM) also reduces the amount of membrane bound and internalized micelles at 37°C. Scale bar = 10 μm. b) Measurements of temperature and free ligand (folic acid) influence on internalization in KB cells. 20%F-60%mix formulation was used. All data shown is in mean±SEM with n>3 individual measurements. c) Rate of increase in cell associated fluorescence for multiple time points after start of incubation with KB cells for all formulations.
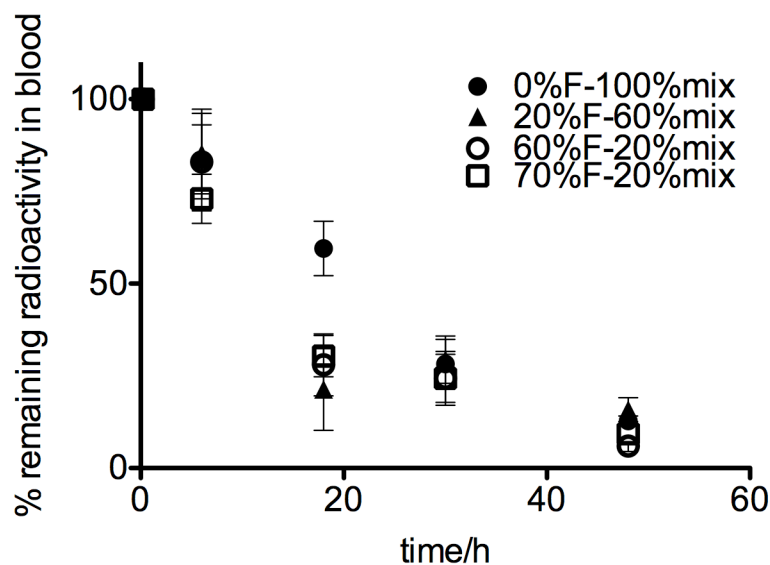
Supplementary Figure 6. Blood circulation of micelles (^{111}In labeled) used for *in vivo* testing. Blood circulation half lives of micelles are between 15 to 20 h.
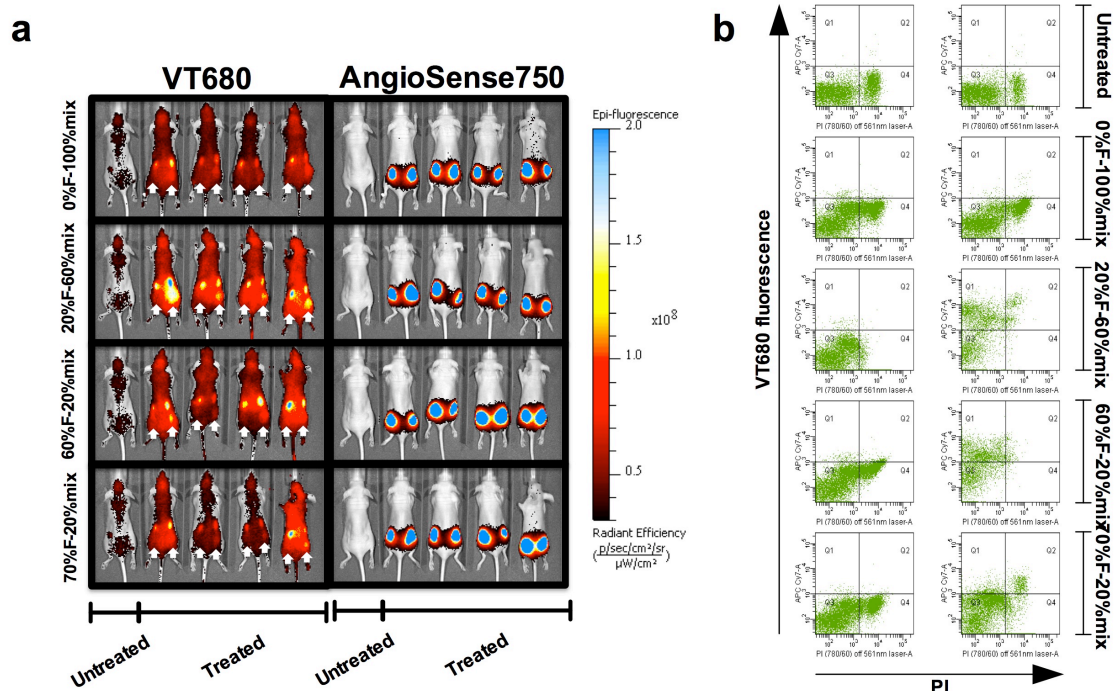
Supplementary Figure 7. a) AngiosSense750 fluorescence from nude mice tumors used to normalize micelle fluorescence to account for size and vasculature differences. Whole body VT680 fluorescence is also shown to allow comparison and tumor identification. b) Flow cytometry analysis of tumor cells isolated from nude mice given the four formulations (n=3, additional raw scatter plots not shown). Untreated cells were from mice not given any injection but stained with PI. Each representative raw scatter plot show cells from one tumor. KB tumors from mice injected with 20%F-60%mix showed the highest percentage of cells above the gated threshold

mean (Q1, top left) and the highest average micelle fluorescence from live cells (Q1+Q3, top left + bottom left). Q1 percentages are 1.2±0.5%, 0.5±0.1%, 0.8±0.4% and 1.0±0.8% for A375 tumors and 2.0±1.4%, 40.1±8.5%, 33.1±7.2% and 21.9±16.2% for KB tumors (0%F-100%mix, 20%F-60%mix, 60%F-20%mix and 70%F-20%mix respectively). Average Q1+Q3 micelle fluorescence is shown in Figure 5d.